Available online at www.sciencedirect.com
ScienceDirect
Catalysis Today 137 (2008) 489–492
CATALYSIS TODAY
www.elsevier.com/locate/cattod

The influence of the Cr–Al foil texture on morphology of adhesive Al_2O_3 layers in monolithic environmental catalysts

A. Białas [a,*], W. Osuch [b], W. Łasocha [a], M. Najbar [a]

[a] Department of Chemistry, Jagiellonian University, Ingardena 3, 30 060 Cracow, Poland
[b] Faculty of Metals Engineering and Industrial Computer Science, University of Science and Technology, Mickiewicza 30, 30-059 Cracow, Poland

Available online 1 April 2008

Abstract

The FeCrAl-alloy foils of 0.1 and 0.05 mm thickness, being the supports of metallic monolithic environmental catalysts, were investigated by XRD and TEM to determine the reasons of the differences in morphology of the alumina adhesive layers grown during oxidation. Alumina adhesive layers of stable thickness and outgrowing scale-like crystallites were observed on 0.1 mm foil and alumina layers of different thickness with lower population of outgrowing scale-like crystallites on 0.05 mm foil. αFe was found to be the only phase seen by XRD in both kinds of the foil. The density of dislocations on the surface of 0.1 mm foil was found to be of one order of magnitude higher than this on the surface of the 0.05 mm one. Both kinds of the foil reveal different texturing investigated with X-ray. Different texturing connected with various face development results in various possibilities of growing Al_2O_3 layers. However, the high dislocation density is responsible for the high population of scale-like crystallites on 0.1 mm foil.

Keywords: Metallic monoliths; FeCrAl-alloy foil; αFe crystallites; Texturing; Dislocation density; Oxidation; Alumina adhesive layer

1. Introduction

Environmental catalysts used in cars are supported on ceramic or metallic monoliths [1–3]. Catalysts used for the purification of off-gases from the stationary sources are usually deposited on ceramic monoliths. However, there are numerous patents concerning those catalysts on kanthal and FeCrAl-alloy foils [4–8]. Car-catalysts deposited on metallic carriers are more convenient within cities; they quickly achieve the onset temperature due to good thermal conductivity of metals. Application of thin foil allows to increase the ratio of channels to walls' volumes. There is an effort to build the monoliths using foil as thin as possible. The Cr–Al stainless steel foils with the thickness of 0.1 mm is commonly used for production of car-monoliths. They contain, beside iron, chromium and aluminum a small addition of yttrium (FeCrAl-alloy) or cobalt (kanthal). On these alloys alumina layers can grow making them adhesive to catalytically active components [3,9–11]

Under oxidizing conditions at high temperatures aluminum segregates continuously to the surface forming an alumina layer. On one hand, such a layer protects the inner part of the monolith against oxidation; on the other hand, the crystallographic misfits between the oxide and alloy as well as the difference in the thermal expansion coefficients of oxide and metal cause strains which can result in the monolith damage, particularly during cooling [9–12]. An increase of aluminum content in the alloy could enhance the monolith thermal durability, especially built of thin foil −0.02 mm, but it is expensive and makes the steel brittle [13]. Since automotive catalysts are more vulnerable to mechanical shocks than thermal one [14] such an improvement is not applied.

Cold rolling of ferritic alloys causes the formation of elongated fine crystallines, such obtained materials show high hardness, which increases with the temperature of treatment attaining the maximum at 748 K. The increase of the temperature to 823 K causes FeCrAl-alloy plasticity and recrystallization resulting in a coarse grained alloy. The hardness is also influenced by the stress; it increases with the increase of pressure [15]. During thermal treatment of FeCrAl-alloys at about 773 K, domains enriched in iron or chromium begin to form, then to the Fe rich domains aluminum segregates [16].

* Corresponding author. Tel.: +48 1266 32242; fax: +48 1263 40515.
E-mail address: anbialas@chemia.uj.edu.pl (A. Białas).

0920-5861/$ – see front matter
doi:10.1016/j.cattod.2008.02.011

The method of the formation of adhesive alumina layers, composed of uniform thickness of alumina layers and outgrowing scale-like crystallites able to hold a wash-coat on 0.1 mm FeCrAl-alloy foil, was ascribed earlier [9,11]. The same method cannot be applied for the obtainment of an adhesive Al_2O_3 layer on the 0.05 mm foil. The thickness of alumina layers formed by this method on 0.05 mm foil is different in different foil areas and scale-like crystallites are much rarer [10]. The morphology of the adhesive alumina layer is thought to depend on the foil structure. To understand the reasons of the difference in the morphology of alumina on 0.1 and 0.05 mm foil and assess the possibility of the formation of the Al_2O_3 layer of high adhesion on 0.05 mm foil the investigation of two kinds of the foil by X-ray diffraction (XRD) and transmission electron microscopy (TEM) was undertaken.

2. Experimental

Stainless steel FeCrAl-alloy foil (Fe:Cr:Al = 74:20:5 wt.%), with the thickness of 0.1 and 0.05 mm (produced in 1993) by A.S. THEIS Stahltechnologie Hagen-Holden, Germany was used for investigations [17].

Phase composition and the crystallites' texturing were determined with X-ray diffraction. A Philips Analytical PW 3710 XPERT System with CuKα ($\lambda = 0.1541$ nm) radiation (40 kV, 30 mA) and secondary beam monochromator at 0.02° steps at the rate of 2 s per step over the range $20^\circ < 2\theta < 100^\circ$ was used to record XRD patterns. Two mutually perpendicular orientations of the foil were tested. The foil was stuck to the upper surface of a sample holder. During the measurement, performed in Bragg–Brentano geometry, the sample was not rotated. After the first measurement the sample was rotated by 90°, and the measurement was repeated.

The defect structure and carbide inclusions were examined by TEM. The TEM images were taken with a JEM 100 C JEOL electron microscope. The foil was thinned to the thickness transparent for electrons by jet electropolishing before the investigation.

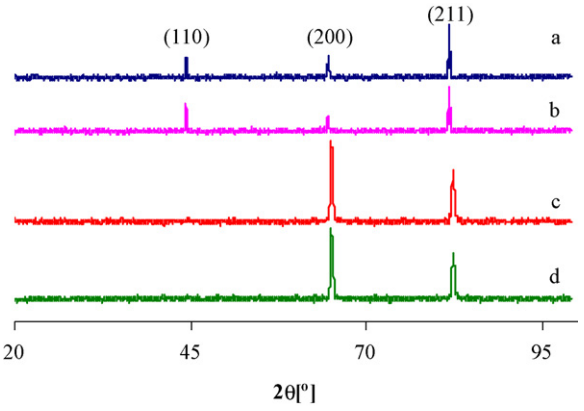

Fig. 1. XRD patterns of: 0.1 mm foil (a), 0.1 mm foil with perpendicular orientation with respect to the previous one (b), 0.05 mm foil (c) and 0.05 mm foil with perpendicular orientation with respect to the previous one (d).

3. Results and discussion

In Fig. 1 the XRD patterns of: 0.1 mm foil (a), 0.1 mm foil with perpendicular orientation with respect to the previous one (b), 0.05 mm foil (c) and 0.05 mm foil with perpendicular orientation with respect to previous one (d) are presented. The positions of all the peaks in the XRD patterns of both kinds of the foil fit very well with those of αFe. Thus, one can conclude that the chromium–iron alloy with the αFe structure is the only phase seen in the both kinds of foil by the XRD. However, the sequences of the reflection intensities in both cases are different. They also differ from the published ones for αFe [18–20].

In Table 1 interplanar distances (d) and relative peaks intensities (I) in the XRD pattern of 0.1 mm foil, taken for two perpendicular foil orientations are compared with one of the data sets for αFe [18].

The observed dependence of the peak intensity sequence on the foil orientation shows texturing the elongated fine αFe crystallites [15] as a result of low temperature foil rolling [17]. This kind of texturing causes exposition of the determined faces on the foil surface and their determined orientation forced by

Table 1
The comparison of the interplanar distances (d) and relative intensities (I) of the peaks in XRD pattern of the 0.1 mm foil of two perpendicular orientations with those in one of published patterns for αFe [18]

$h\,k\,l$	I αFe [18] (%)	d αFe [18] (Å)	I foil (%)	I foil$_\perp$ (%)	d foil (Å)
(1 1 0)	100	2.03	35	62	2.04
(2 0 0)	20	1.43	43	32	1.44
(2 1 1)	30	1.17	100	100	1.18

Table 2
The comparison of the interplanar distances (d) and relative intensities (I) of the peaks in XRD pattern of the 0.05 mm foil of two perpendicular orientations with those in one of published patterns for αFe [18]

$h\,k\,l$	I αFe [18] (%)	d αFe [18] (Å)	I foil (%)	I foil$_\perp$ (%)	d foil (Å)	d foil$_\perp$ (Å)
(1 1 0)	100	2.03	3	4	2.04	2.03
(2 0 0)	20	1.43	100	100	1.43	1.43
(2 1 1)	30	1.17	67	65	1.17	1.17

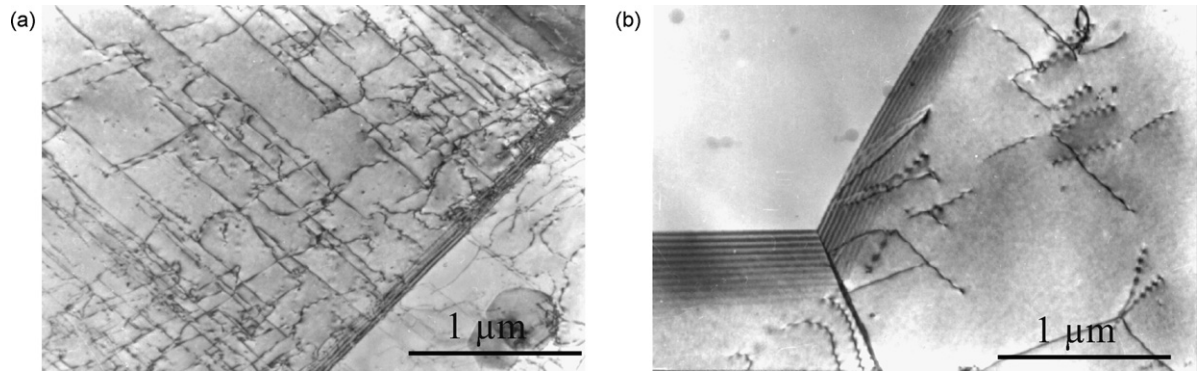

Fig. 2. TEM micrographs of 0.1 mm (a) and 0.05 mm foil (b).

Table 3
Dislocation density

Foil thickness (mm)	Dislocation density (D.N. m^{-2})
0.1	2.8×10^{14}
0.05	4.5×10^{13}

the rolling direction. Similar rate of aluminum segregation on the exposed faces of all the steel crystallites results [9,11] in the formation of the alumina layers of the similar thickness on the foil surface.

In Table 2 the interplanar distances and relative peak intensities in the XRD patterns taken from two perpendicular 0.05 mm foil orientations are compared with those of αFe [18]. Independence of the peak intensity sequence of the foil orientation with respect to X-ray direction shows lack of the preferential crystalites' orientation as a result of foil rolling. It is caused by recrystallization resulting in coarse grains' formation at temperatures above 823 K, as it was observed by Chao and Gonzalez-Carrasco [15]. The differences in the alumina layers' thickness in particular areas of the 0.05 mm foil can easily be explained if remember that at ca 773 K the domains enriched in iron and aluminum or in chromium are formed [16]. It is obvious that the alumina layers on the domains enriched in Fe and Al are thicker than the ones on Cr enriched areas.

The above-discussed XRD results, confirm that the method of foil rolling determines αFe crystallites' shapes [15] and also reveal that it influences crystallites' orientation.

In Fig. 2 typical examples of TEM micrographs of 0.1 mm (a) and 0.05 mm (b) foil are presented. As seen, crystallites of 0.1 mm foil contain numerous dislocations. On the other hand, the number of dislocation in crystallites of 0.05 mm foil is much smaller.

The number of dislocations for the both kinds of the foil was calculated from the equation:

$$\rho = \frac{x \cdot 2 \cdot N}{L \cdot t}$$

where ρ is the dislocation number, L the length of secant, N the number of dislocations crossing with secants, x the factor describing the number of invisible dislocations with Burger's vector $a/2\langle 1\ 1\ 1\rangle$ and t is the foil thickness.

The dislocation densities for both kinds of the foil are presented in Table 3.

In 0.1 mm foil the dislocation density is equal to 2.8×10^{14} D.N. m^{-2} and is six times greater than in the 0.05 mm foil. It can be expected that growth of Al_2O_3 on the dislocations is responsible for scale-like crystallites growing out from the surface of 0.1 mm foil. However, Al_2O_3 growth on the exposed face of αFe crystallite causes the formation of an Al_2O_3 layer. The difference in the number of dislocations can also be ascribed to the various methods of foil rolling. It can be expected that due to low steel plasticity at ambient temperature, rolling causes the big strains in αFe crystallites resulting in the formation of numerous dislocations. However, higher steel

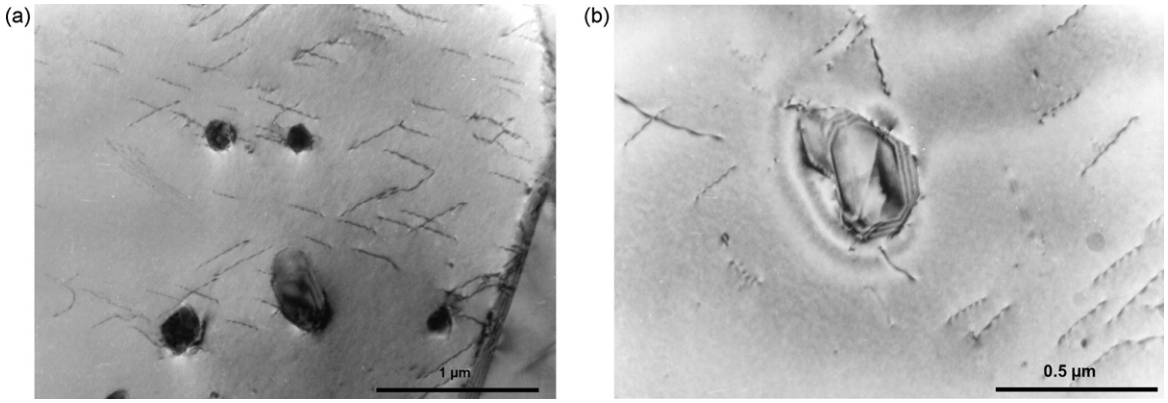

Fig. 3. TEM micrographs of the 0.1 mm (a) and 0.05 mm (b) foil with iron carbide inclusions.

plasticity at 873 K causes smaller strains in αFe crystallites resulting in a smaller number of dislocations.

In Fig. 3 the TEM micrographs of the 0.1 and 0.05 mm foil with iron carbide inclusions are presented. The presence of carbide crystallites of similar dimensions in both kinds of the foil is understandable if take into account that carbides are formed above 973 K. The similarity of the shape and population of carbide crystallites in both kinds of the foil excludes their responsibility for the difference in alumina layer morphology. Hence, one can imagine that during foil oxidation carbide inclusions in the foil subsurface layers disappear due to oxidation-induced surface carbon segregation.

4. Conclusions

Alumina adhesive layers of stable thickness and outgrowing scale-like crystallites were earlier observed on cold rolled 0.1 mm foil and alumina areas of different thickness with smaller amounts of outgrowing scale-like crystallites on 0.05 mm foil rolled at ca 873 K. The surface containing a high population of scale-like crystallites is very adhesive for the alumina wash-coat. The XRD and TEM measurements were performed to investigate the reason of the difference in alumina layers morphology on both kinds of the foil.

On the basis of the XRD measurements it was stated that αFe is the dominating phase in FeCrAl-alloy foil with the thickness of 0.1 and 0.05 mm. The peak intensity sequence in the XRD patterns of both kinds of foil is different and in the case of 0.1 mm foil it depends on the foil orientation. It means that the method of foil rolling determines the shape and orientation of the αFe crystallites. The TEM images have revealed that 0.1 mm foil is built of crystallites with a higher dislocation density while 0.05 mm foil is composed of the less defected crystallites. It was shown that the thickness of alumina adhesive layer grown on αFe crystallites is determined by the aluminum content in the foil domains. However, the density of the dislocations is responsible for the population of the scale-like crystallites, which grow out from alumina layer.

Acknowledgement

This paper was supported by Polish Committee of Scientific Research, Grant BPZ-KBN-116/T09/2004 and by EUREKA E! 3230 STATIONOCAT.

References

[1] J.L. Williams, Catal. Today 69 (2001) 3.
[2] R.M. Heck, S. Gulati, R.J. Farrauto, Chem. Eng. J. 82 (2001) 149.
[3] P. Avila, M. Montes, E. Miro, Chem. Eng. J. 109 (2005) 11.
[4] L. Chapman, US patent 4,318,828 (1982).
[5] L. Chapman, C. Vigor, J. Watton, US patent 4,331,631 (1982).
[6] G. Aggen, P. R. Borneman, US patent 4,414,023 (1982).
[7] K. Lindsey, US patent 4,782,039 (1988).
[8] W. R. Alcorn, US patent 4,912,776 (1990).
[9] M. Najbar, A. Steiner, A. Białas, E. Bielańska, J. Camra, Polish Patent 183,563,(2002).
[10] J. Camra, E. Bielańska, A. Bernasik, K. Kowalski, M. Zimowska, A. Białas, M. Najbar, Catal. Today 105 (2005) 629.
[11] B. Pietruszka, M. Najbar, L. Lityńska-Dobrzyńska, E. Bielańska, M. Zimowska, J. Camra, Stud. Surf. Sci. Catal. 136 (2001) 471.
[12] M. Schutze, W. Przybilla, Metal-supported automotive catalytic converters, in: H. Bode (Ed.), Werkstoff InformationsgesellschaftmbH (1997) 163.
[13] J.R. Nicholls, W.J. Quadakkers, in: H. Bode (Ed.), Materials Aspects in Automotive Catalytic Converters, Wiley-VCH, Weinheim, 2002, p. 31.3.
[14] S. Zhao, J. Zhang, D. Weng, X. Wu, Surf. Coat. Technol. 167 (2002) 97.
[15] J. Chao, J.L. Gonzalez-Carrasco, Scripta Mater. 50 (2004) 1457.
[16] H.G. Read, H. Murakami, Scripta Mater. 36 (1997) 355.
[17] A. Steiner, private information.
[18] PDF 06-0696.
[19] PDF 01-1262.
[20] PDF 03-1050.